KFUPM
Journal of Undergraduate Research International

Diamond Open Access 152

Article Mechanical Engineering

Development and Characterization of Sustainable Form-Stabilized Phase-Change Materials Incorporating Industrial Waste for Battery Thermal Management Applications

Meshal Alghamdi and Obaidallah Munteshari*

Cite https://doi.org/10.64589/juri/231574

Submitted: April 23, 2026 **Revised:** May 10, 2026 **Accepted:** May 17, 2026

ABSTRACT

The need for reliable thermal management strategies has intensified with the rapid growth of lithium-ion batteries in electric vehicles, particularly in hot climates where high ambient temperatures accelerate degradation, reduce efficiency, and increase safety risks. Owing to their high latent heat of storage and ability to maintain stable temperatures, phase-change materials (PCMs) are promising candidates for passive cooling. However, leakage issues and the low thermal conductivity of PCMs limit their practical application in battery thermal management. This study presents a sustainable form-stabilized PCM (FS-PCM) developed using paraffin RT42 mixed with oil ash (OA), an industrial waste material, in a controlled environment. The composite prepared via vacuum impregnation of 45 wt.% RT42 and 55 wt.% OA demonstrated structural stability with retained crystal structure, as confirmed by X-ray diffractometry. Thermal analysis revealed a melting temperature of 33.8 °C and a latent heat of 81.5 J/g, indicating its suitability for battery thermal regulation. The PCM was encapsulated within the porous OA matrix and exhibited a uniform elemental distribution, as revealed by microstructural characterization. Application of the FS-PCM significantly enhanced battery thermal management by lowering the maximum temperature increase to 7.25 °C at a discharge rate of 4C and maintained temperature uniformity within safe limits (<5 °C) at an FS-PCM thickness of 7 mm. Overall, the developed FS-PCM offers a cost-effective, sustainable, and efficient solution for passive battery cooling in high-temperature environments.

Keywords: thermal management, Li-ion battery, phase change materials, oil ash, material characterization

1. INTRODUCTION

Driven largely by global efforts to reduce carbon emissions, the adoption of lithium-ion batteries (LIB) as cleaner alternatives to fossil fuels has grown substantially in the past few decades [1,2]. Internal combustion engines, particularly diesel-powered vehicles, are significant contributors to NO_x emissions and air pollution [3,4], and the greenhouse gases released drive climate change via atmospheric heat retention [5]. Therefore, transitioning to electric vehicles (EVs) powered by LIBs is widely recognized as a critical step toward achieving sustainability goals [6], as EVs produce no direct exhaust emissions and demonstrate lower lifecycle greenhouse gas emissions than conventional diesel vehicles [7–9]. However, EV performance is strongly influenced by regional environmental conditions [10,11]. For instance, Saudi Arabia presents a particularly challenging environment, with summer temperatures regularly reaching 40 °C and occasionally exceeding 45 °C [12–15]. These conditions are compounded by intense solar radiation and frequent dust storms that impose significant thermal loads on battery systems [16,17]. Within Saudi Arabia's Vision 2030 framework, which prioritizes sustainability and carbon footprint reduction [18,19], addressing the thermal adaptability of EVs in hot, arid climates is essential [20]. Indeed, the combination of elevated ambient temperatures with internal heat generation during vehicle operation accelerates battery capacity degradation and shortens the operational lifespan [21]. Although lead–acid and nickel-based batteries have been used historically, their considerable weight and limited cycle life restrict their suitability for modern EV applications [22–25]. Contrastingly, LIBs offer superior energy density, lightweight design, and reliable cycling performance, rendering them the dominant technology in the current EV market [26–29]. Nevertheless, their performance and safety are dependent on thermal conditions [30–32], requiring operation within an optimal temperature range (15–35 °C) [33]. Exceeding this range accelerates degradation, impairs performance, and raises safety concerns, including thermal runaway [34,35]. Such risks are amplified as EV deployment continues to expand globally [36].

Battery thermal management systems (BTMSs), including air cooling, liquid cooling, refrigerant-based methods, and heat pipes, have been extensively explored [37–39]. The simplest BTMS is the air cooling system; however, its use is limited to high-temperature climates [40,41]. On the other hand, liquid cooling enhances heat dissipation but also increases system complexity

Published under an exclusive license by KFUPM

and overall energy consumption[42]. Although refrigerant-based cooling systems can effectively reduce battery temperatures, they also introduce additional energy requirements[43,44]. Accordingly, for high-temperature environments, passive thermal management systems provide a clear advantage because they control high temperatures and require no external energy[30–32].

Among the various passive cooling approaches, phase-change materials (PCMs) have gained significant attention[45,46]. These materials absorb and release heat during phase transitions, helping maintain nearly constant temperatures around the battery cells[47–49]. Extensive studies have confirmed that paraffin wax, polyethylene glycol, and commercial RT-series paraffin wax PCMs can successfully lower the maximum battery temperature while improving the overall temperature uniformity[50–52]. However, despite these advantages, conventional PCMs suffer from inherently low thermal conductivity and leakage problems, which limit their application in BTMSs[53,54]. To overcome these drawbacks, various form-stabilized PCMs (FS-PCMs) have been developed that incorporate conductive materials, such as graphene and metal foams, to accommodate melted PCMs without leakage, while also exhibiting enhanced thermal conductivity and performance[55]. Additionally, Xin et al.[56] experimentally and numerically demonstrated that a hybrid BTMS combining a composite PCM with liquid cooling effectively controlled the maximum battery temperature at 48.97 °C and maintained a temperature difference of <4.5 °C even under a 2C discharge rate at an ambient temperature of 37 °C. Previous studies have primarily focused on high-cost nano-enhanced PCMs or metallic foams, with limited attention being paid to low-cost industrial waste integration[57,58]. However, the use of high-cost porous carbon materials often increases system costs and manufacturing complexity, limiting the large-scale production of these systems. Accordingly, it is important to employ sustainable, cost-effective solutions for the use of waste materials in thermal management applications[59]. Consequently, Ping et al.[60] developed a nano-encapsulated inorganic PCM by incorporating $Na_2HPO_4 \cdot 12H_2O$ within a silica matrix, achieving 23.7% peak temperature reduction at a 3C discharge rate while simultaneously suppressing thermal runaway and eliminating the fire hazards associated with conventional organic PCMs. Additionally, Al Miaari et al.[61] developed an FS-PCM that incorporated waste ash for photovoltaic (PV) thermal management. They demonstrated that oil ash (OA) could be used as a supporting material to develop an FS-PCM for passive PV cooling. The prepared FS-PCM exhibited outstanding thermophysical properties, rendering it a suitable candidate for PV thermal management[61]. This confirms

Table 1. *Comparison of different PCMs applied in the thermal management of batteries*

PCM	T_m (°C)	ΔH_m (J/g)	T.C. (W/m · k)	Charge/ Discharge rate	Max. temp. reduction (°C)	Limitations	Ref.
RPCM	52.89	157.5	2.0	2C	9.11	Lower flame retardancy	62
Paraffin	58	195.7	-	-	-	Uneven melting; slow cooling; Although adding fins extended the operating time to 1600 s (compared to 1200 s for PCM alone), it increased the system weight and geometric complexity.	63
PCM-EG10@SEBS	36.55	101.9	6.55	1.5C	18.8	Conductivity loss after cycling	64
Pure paraffin wax	61.46	278.4	-	3C	10.9	Low thermal conductivity; slow melting; uneven temperatures	65
RT35HC paraffin	34	186	-	2C	9	Partial solidification at 2C	66
RT35 paraffin	30	179	0.2	1C, 2C, and 3C	30	Low thermal conductivity; PCM underutilization	67
Palm fatty acid distillate	32.21	82.5	0.23	0.27C, 0.56C, 0.83C	7.9	Low latent heat; low thermal conductivity	68
Lauric acid + stearic acid	33.29	151.8	0.36	1C, 1.5C, 2C	Reduced to 34.5 °C (1C), 36.7 °C (1.5C), 39.5 °C (2C)	Longer solidification at high C-rates; the performance is sensitive to ambient temperature fluctuations	69
Paraffin	40	137	0.2	1C, 2C, 3C	ΔT: 6.0 °C (vs. pure PCM, at 60% Depth of Discharge, 3C)	PCM flow after melting causes nonuniformity	70
PEG	43.95	118	1.34	3C	ΔT: 3.55–5.08 °C	Performance highly dependent on filled configuration	71

the potential of using OA for additional thermal management applications, such as BTMSs.

Despite these advances in the use of OA as a porous supporting matrix for PCMs in PV thermal management, the operating requirements of PV cooling differ substantially from those of lithium-ion BTMSs, and a PCM formulation tuned for one application is not directly transferable to another. For instance, PV modules generate a quasi-steady heat flux driven by solar irradiance, typically demanding PCM melting temperatures of 50–70 °C and accommodating slow diurnal thermal cycles. Contrastingly, LIBs operate within a significantly narrower safe operating window of 15–35 °C. Additionally, they produce transient, rate-dependent heat during high C-rate discharge and require strict control over temperature uniformity, tolerance to leakage under repeated melt–solidification cycles, and close, conformal contact with cell surfaces.

The aim of this study is therefore to optimize the RT42/OA composition, which employs the verified structural stabilization characteristics of oil as[61], and vacuum-impregnation loading ratio for application in LIBs. To the best of our knowledge, no previous studies have developed or experimentally validated an OA-supported FS-PCM for LIB thermal management, particularly under the elevated ambient temperatures characteristic of hot arid climates. Therefore, the present work extends the use of OA valorization into a distinct and more demanding thermal-management regime, while addressing the leakage and low thermal-conductivity limitations of pure paraffin. To improve the heat-dissipation capability of pure PCMs, traditional systems often incorporate fins—metallic extensions that boost heat transfer. Although fins work well, they add extra weight and making the system bulkier. Table 1 compares recently published studies on the implementation of PCMs for the thermal management of batteries with different battery types and application locations.

2. METHODOLOGY

2.1. Materials. To prepare the target FS-PCM, RT42 paraffin wax (Rubitherm Technologies GmbH, Germany) was impregnated into OA via a two-step vacuum impregnation method; raw OA powder was evacuated at 80 °C for 1 h, and liquid RT42 was introduced under vacuum for 2 h to ensure full pore penetration. The latent heat, melting point, and thermal conductivity of RT42 are 178 kj/kg, 38 °C, and 0.2 W/(m · K), respectively[72]. OA with a carbon content of >90 wt.% was obtained from the Saudi Electricity Company (Saudi Arabia).

2.2. Characterization. The crystalline phases and mineral composition of the samples were analyzed using X-ray diffractometry (XRD, Rigaku) at 30 kV and 15 mA, employing Cu-Kα radiation with a scan speed of 2°/min. The surface morphology and microstructural features were investigated using field-emission scanning electron microscopy (FE-SEM, JEOL JSM-6400F) at an accelerating voltage of 10 kV. The elemental composition and distribution were further examined via energy-dispersive X-ray spectroscopy (EDS) combined with SEM. The thermal properties were evaluated using differential scanning calorimetry (DSC). The sample (~10 mg) was sealed in an aluminum pan and heated at a rate of 5 °C/min under a continuous flow of argon (20 mL/min). The thermal conductivity of the FS-PCM composite was measured using a FOX 50 heat flow meter, offering a temperature resolution of ±0.01 °C and a measurable thermal resistance range of 0.003–0.05 $m^2 \cdot K/W$.

Table 2. *Weight variation and leakage assessment of the FS-PCM samples after thermal exposure*

Sample	Weight before heating (g)	Weight after heating (g)	Weight loss (%)
30 wt.% RT42	1.51	1.50	0.66
40 wt.% RT42	1.55	1.54	0.65
45 wt.% RT42	1.48	1.47	0.68
50 wt.% RT42	1.50	1.33	11.33

3. FS-PCM PREPARATION AND LEAKAGE TEST

The FS-PCM composite was prepared using a controlled vacuum impregnation technique to ensure the effective incorporation of RT42 into the porous OA matrix. Initially, different mass fractions of RT42 and OA were added to clean glass beakers. These mixtures were then heated at 60 °C under magnetic stirring at 300 rpm for 30 min to fully melt the paraffin and promote uniform OA dispersion within the liquid phase. Continuous mixing was maintained to enhance interactions between RT42 and the porous OA structure. Subsequently, the mixture was transferred to a vacuum oven and subjected to vacuum impregnation at 0.10 MPa and 80 °C for 2 h. This step facilitated the penetration of molten paraffin into the interconnected pore structure of OA by removing trapped air and enhancing capillary absorption.

Following impregnation, the prepared FS-PCM was removed from the oven and was allowed to cool naturally to a controlled laboratory temperature of 25 ±2 °C. The solidified composite was then collected and mechanically compressed into disk-shaped samples using a hydraulic pressing machine to obtain a uniform geometry and enhance structural integrity.

A leakage test was conducted on the FS-PCM composite to evaluate the shape stability and leakage resistance. The pressed samples were placed in an oven for 30 min at 80 °C, which exceeded the melting temperature of RT42. The samples were visually inspected after heating to assess for any signs of paraffin leakage, and the weight loss of each sample was recorded (Table 2). For RT42 loadings ≤45 wt.%, sample weight loss was negligible. However, a significant increase in weight loss was observed at 50% RT42, indicating leakage from the OA medium. Accordingly, 45 wt.% was selected as the optimal RT42 content for further investigations.

4. RESULTS AND DISCUSSION

4.1. XRD. XRD was performed to examine the crystalline structure and unit cell characteristics of the synthesized FS-PCM, revealing highly crystalline phases (Figure 1)[73]. Scanning was performed over a 2θ range of 5°–80°, with a step size of 0.01°and a scan rate of 3°/min. Distinct diffraction peaks were identified for OA, with a major reflection at a 2θ angle of ~26°(101), corresponding to SiO_2, while another notable peak at ~43.1°(202) was attributed to $CaCO_3$. The XRD profile of RT42 confirms its

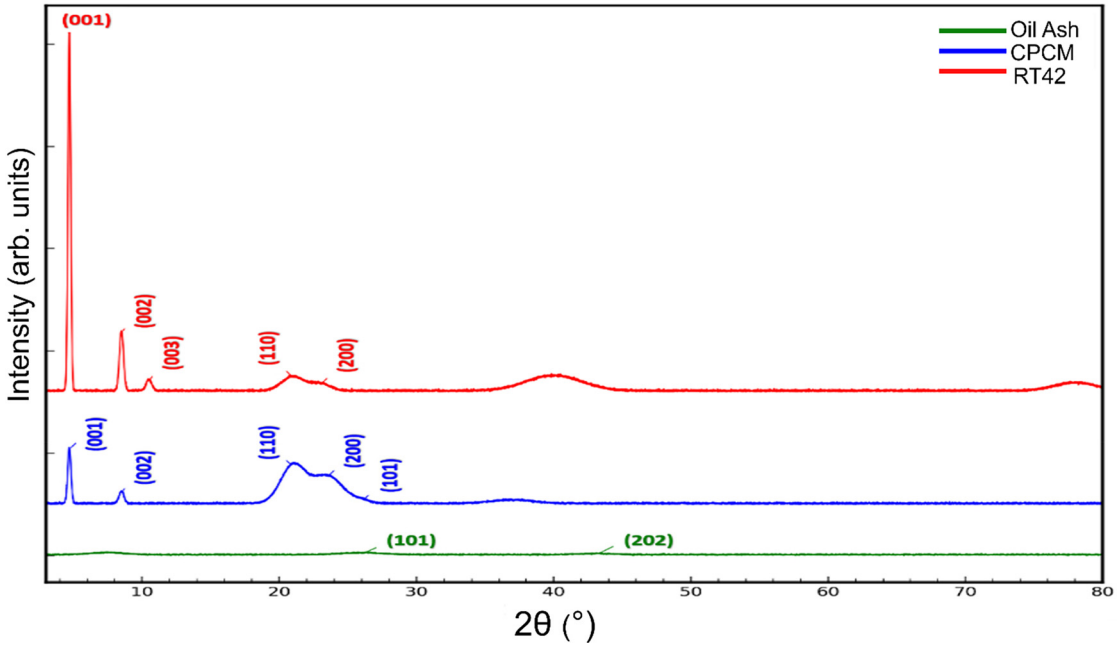


Figure 1. XRD patterns of the RT42, OA, and FS-PCM specimens

highly crystalline structure[73], characterized by two sharp peaks located at 21.2°and 23.2°, which correspond to the (110) and (200) crystal planes of paraffin wax. The observation of comparable peaks for the FS-PCM sample indicate that the incorporation of OA did not alter the RT42 crystal structure, suggesting that composite formation occurred without chemical transformation. Phase identification and peak indexing were performed using X'Pert HighScore software in conjunction with the JCPDS reference database.

4.2. DSC. To examine the thermal behavior of the prepared samples[74], DSC measurements were performed between 0 and 100 °C, with a controlled heating rate of 5 °C/min. A steady flow of nitrogen gas was maintained to avoid sample oxidation[75]. The latent heats of the materials were determined by integrating the areas under their corresponding DSC curves[76]. As shown in the resulting thermograms (Figure 2), the thermal transitions are fully reversible under the investigated conditions[76]. In the endothermic region, the melting peak temperature was recorded as 33.8 °C and the corresponding latent heat was 81.5 J/g, representing a reduction compared with that of the pure RT42 (i.e., ~178 J/g). This ~54% reduction can be attributed to the presence of the thermally inert OA[61], which accounts for ~55% of the total mass and consequently lowers the proportion of active PCM compared with that in the pure RT42. Notably, this reduction is an inherent and unavoidable consequence of form-stabilization rather than representing PCM degradation. These findings confirm that RT42 retains its full latent heat capacity on a per-unit-paraffin basis. A comparable tradeoff has also been reported for ash- and porous-support-based FS-PCMs, including a PV-oriented OA/RT-31 composite[61], which exhibited a comparably reduced latent heat. Critically, the loss in volumetric storage was compensated for by a substantial gain in heat-transfer performance. Consequently, the current FS-PCM achieved a thermal conductivity of 0.696–0.706 W/m · K versus 0.2 W/m · K for the pure RT42, representing a ~3.5-fold enhancement that enables rapid heat extraction from the cell surface. From a system-level perspective, the relevant figure of merit for the BTMS is not bulk latent heat alone but the ability of the composite to suppress the peak cell temperature and maintain temperature uniformity during transient high-rate discharge. Notably, the FS-PCM reduced the maximum cell temperature (T_{max}) by 7.25 °C at a 4C discharge rate and maintained the temperature difference (ΔT) within the 5 °C safety limit, confirming that the residual latent heat is sufficient for the thermal load imposed by realistic battery duty cycles. Furthermore, leakage tests (Table 2) showed that formulations with higher latent heat, achieved by reducing the support fraction, failed to maintain shape stability when the RT42 content exceeded 45wt.%. Consequently, the present composition represents a deliberate balance between energy storage density, thermal conductivity, and leakage-free operation.

4.3. Morphology and Elemental Composition. The surface morphology of the FS-PCM composite containing 45 wt.% RT42 and 55 wt.% OA (i.e., the 45–55 sample) was examined using SEM. As shown in Figure 3, SEM micrographs captured at different magnifications reveal that the OA particles possess a predominantly spherical shape with a highly porous texture. The pore openings are uniformly distributed, and their diameters typically range in 10–50 μm. These interconnected pores provide sufficient space for molten RT42 to penetrate and disperse within the OA matrix during the impregnation process. Compared with the previously reported 40–60 composite[61], the 45–55 sample exhibited a denser surface and fewer visible voids, suggesting a higher degree of paraffin infiltration. Additionally, the smoother appearance and partial filling of surface pores indicated strong bonding between RT42 and OA. This intimate contact contributes to improved structural integrity, enhanced thermal conductivity, and superior shape stability, while effectively preventing paraffin leakage during the phase transition. The observed morphology confirmed the successful integration of RT42 into the porous OA framework, forming a uniform

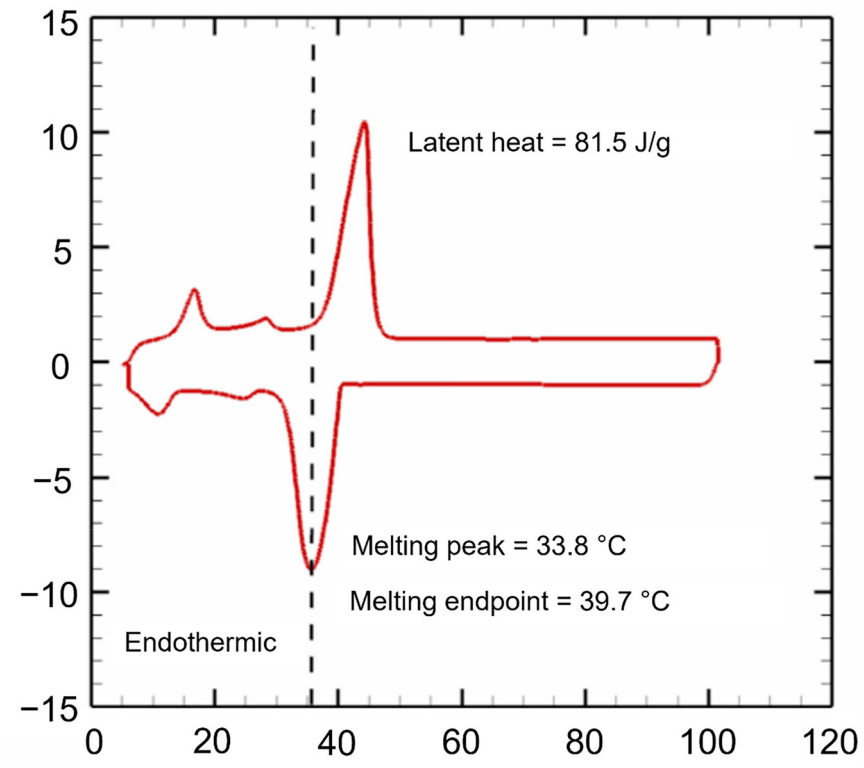


Figure 2. DSC curves recorded for the FS-PCM specimen

and mechanically stable composite suitable for passive battery thermal management.

Subsequently, EDS was employed to investigate the elemental composition and distribution of the 45–55 FS-PCM composite. As shown in Figure 4, the mapping results confirm the presence of C, O, and S as the main elements within the composite. Carbon derived from paraffin RT42 was evenly distributed throughout the structure, indicating uniform dispersion of the PCM within the porous OA matrix. Sulfur, primarily originating from OA, was also widely distributed throughout the sample, suggesting that both components were well integrated at the microscale. The uniform distribution of O was attributed to the minor oxide compounds naturally present in the ash. The overlapping elemental regions further verify that RT42 was successfully impregnated and adhered to the internal pores of the OA particles. This homogenous distribution of elements confirms strong interfacial bonding between the two materials, demonstrating successful composite formation and confirming that OA serves as a stable carrier for the paraffin PCM.

4.4. Thermal Conductivity. To examine the effects of OA addition on the thermal conductivity of RT42, which plays a crucial role in thermal management, thermal conductivity measurements were performed. A cylindrical pellet (20 mm diameter, 15 mm thickness) was placed between the plates of a LASER COMP TA heat-flow meter with side insulation to maintain one-dimensional heat transfer, as illustrated in Figure 5 (a). During the experiment, the temperatures of the upper and lower plates were adjusted to maintain a constant temperature difference of 5 °C. Measurements were performed at several mean plate temperatures, ranging 30–45 °C. Four readings were taken at each temperature and the average values were used to determine the thermal conductivity. The influence of temperature on the average thermal conductivity of the FS-PCM specimen is shown in Figure 5 (b).

4.5. Thermal Performance During LIB Operation. To evaluate the application potential of the prepared FS-PCM, battery thermal management experiments were conducted using a 3000 mAh pouch cell with a nominal voltage of 3.6 V and a cut-off voltage of 2.5 V. The experimental setup illustrated in Figure 6 consists of an environmental chamber (Infitek Co., Ltd., China) with controlled conditions of 20 °C and 50% relative humidity. The battery was tightly encapsulated in the FS-PCM, and the test was conducted under two FS-PCM thicknesses of 5 and 7 mm. The thermal conductivity of the developed FS-PCM was measured at multiple temperatures; specifically, the thermal conductivity was found to be 0.696 W/m · K at 30 °C, 0.701 W/m · K at 35 °C, 0.706 W/m · K at 40 °C, and 0.706 W/m · K at 45 °C. These values represent an enhancement of ~250% compared with that of the pure RT42, which has a thermal conductivity of only 0.2 W/m · K. This substantial improvement was primarily attributed to the high carbon content (>90 wt.%) of the OA matrix, which formed an interconnected thermally conductive network throughout the composite structure, facilitating more efficient heat-transfer.

A battery testing system (Neware Technology Co., Ltd., China) was employed to discharge the cells at a rate of 4C. Prior to testing, the cells were pre-cycled three times at 0.1C to stabilize their electrochemical performance. Two thermocouples (Type-K) were attached at two positions of the cell, one near the tab (7 mm) and the other at a distance of 70 mm from the tab.

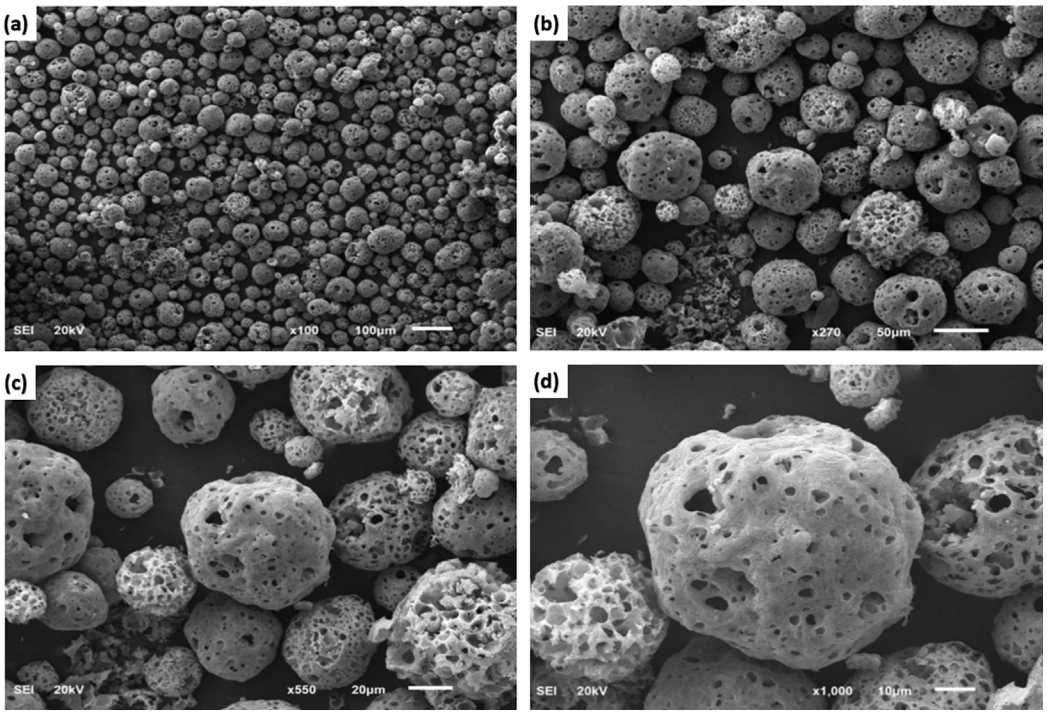


Figure 3. SEM micrographs of the FS-PCM containing 45 wt.% RT42 and 55 wt.% OA at magnifications of (a) ×100, (b) ×270, (c) ×550, and (d) ×1000. The images show a spherical porous morphology and uniform paraffin impregnation within the OA framework

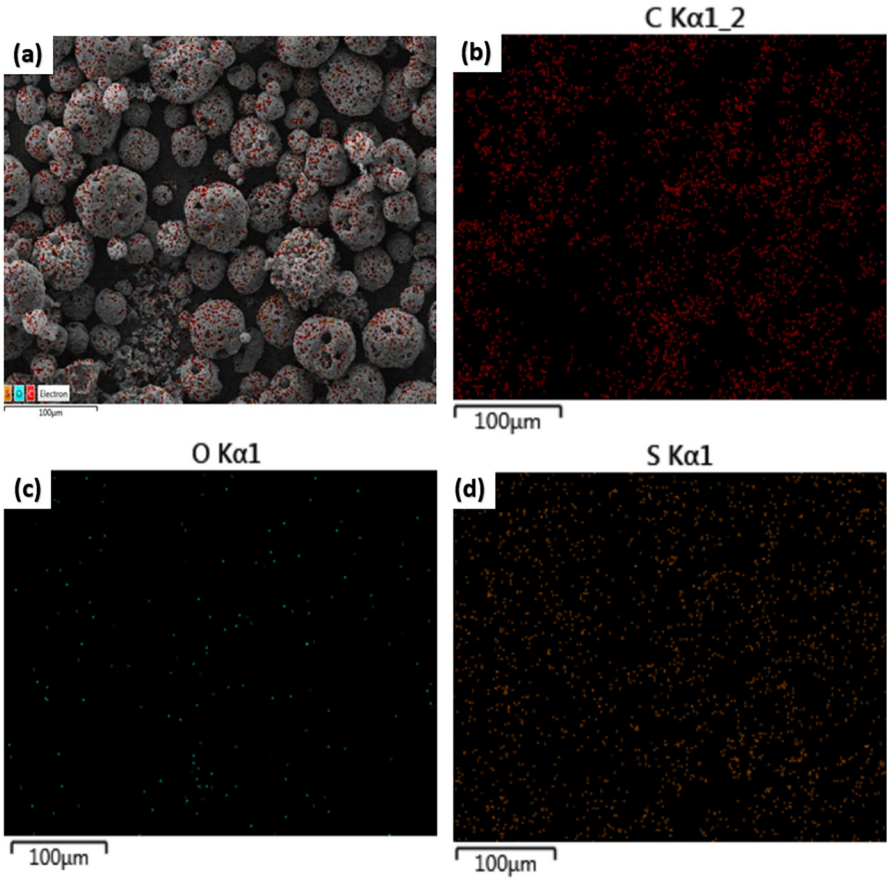


Figure 4. Elemental mapping of the FS-PCM containing 45 wt.% RT42 and 55 wt.% OA showing the distributions of (a) all elements, (b) C, (c) O, and (d) S, confirming the uniform dispersion of RT42 within the porous OA framework

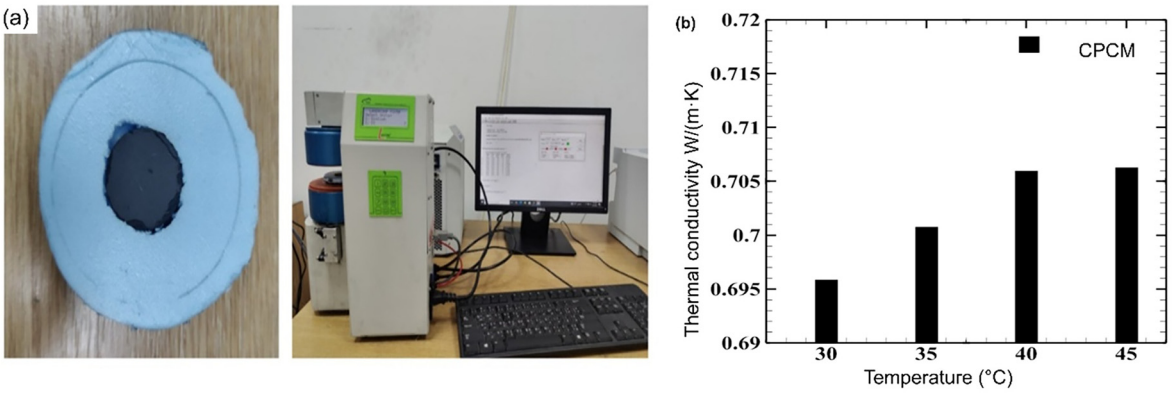


Figure 5. a) The FS-PCM sample and LASER COMP TA heat-flow meter used for the thermal conductivity measurements. (b) Variation of the FS-PCM thermal conductivity with temperature

The thermocouples were connected to a data acquisition system (NI cDAQ-9187) to monitor battery temperature evolution. The thermal performance of the battery was evaluated based on T_{max} and ΔT on the battery surface.

The results reveal a significant improvement in thermal regulation when incorporating the FS-PCM (Figure 7). At a discharge rate of 4C, the T_{max} of the battery containing a 5 mm-thick FS-PCM decreased from 42.35 to 36.78 °C under natural cooling, reflecting a reduction of 5.57 °C, whereas at 3C, T_{max} was reduced from 35.9 to 34.53 °C. Upon increasing the FS-PCM thickness to 7 mm at 4C, T_{max} was reduced to 35.1 °C, representing a reduction of 7.25 °C, whereas at 3C, T_{max} was reduced to 33.43 °C, which is within the safe temperature range. This enhanced performance was attributed to the combined effects of the high thermal conductivity and latent heat storage capacity of the FS-PCM, which facilitate efficient heat absorption and dissipation.

Additionally, the FS-PCM significantly improved the temperature uniformity across the battery surface. Without cooling, ΔT exceeded the safe limit of 5 °C at higher discharge rates, reaching 8.23 °C at 4C and 7.14 °C at 3C. Contrastingly, the FS-PCM maintained ΔT within safe limits, reducing it to 5.72 and 4.65 °C at 4C, and to 5.04 and 4.32 °C at 3C, corresponding to the FS-PCM layer thicknesses of 5 mm and 7 mm, respectively. This improved uniformity is crucial for preventing cell imbalance, overdischarge, and accelerated degradation. Overall, the FS-PCM demonstrated strong potential for enhancing both the thermal safety and performance stability of LIB systems.

The above results can be rationalized by considering that during discharge, Joule heating within the cell is transferred to the surrounding FS-PCM through three sequential mechanisms: (i) conduction from the cell wall into the solid composite, (ii) progressive melting of the paraffin within the OA pore network at its phase-transition temperature of 33.8 °C, and (iii) continued conduction through the partially molten composite after the latent reservoir has been engaged. Below the melting point, heat transfer is governed by Fourier conduction with an effective thermal conductivity of ~0.70 W/m · K, representing a 3.5-fold improvement over that of the pure RT42. This was attributed to the percolating carbon-rich OA network, as confirmed by EDS mapping. Upon the initiation of melting, the latent absorption suppresses the sensible-heating rate, thereby accounting for the inflection observed in the T_{max} profiles and the characteristic temperature plateau at ~34–36 °C. A simple lumped-capacitance estimate based on the heat-generation rate of the cell at 4C (i.e.,

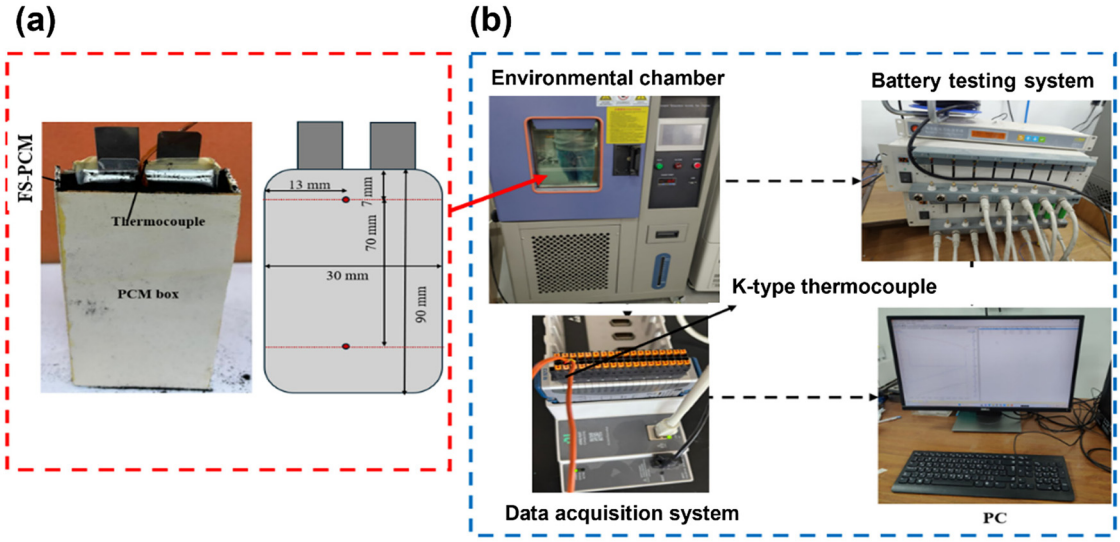


Figure 6. a) Schematic representation of the battery module and (b) the experimental BTMS setup

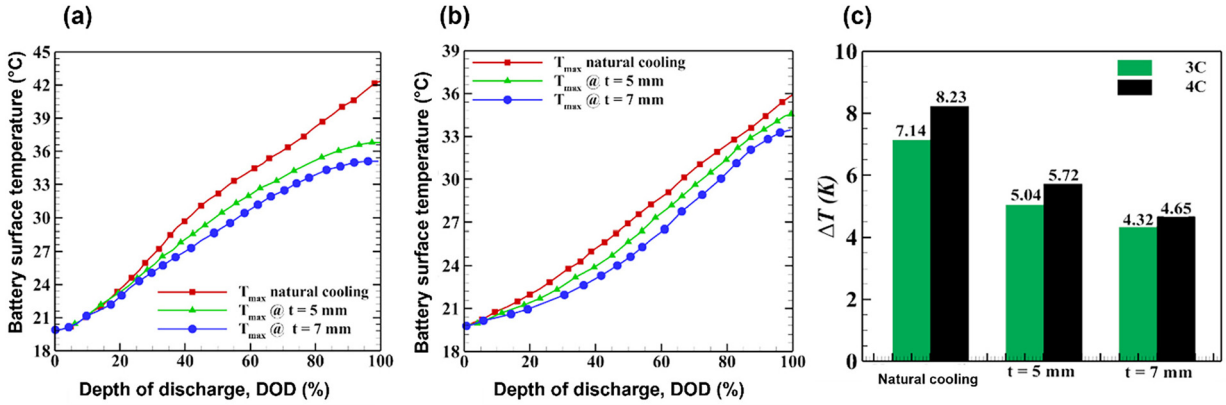


Figure 7. Thermal behavior of the battery with and without FS-PCM cooling at different thicknesses, showing the variations (a) T_{max} at 3C, (b) T_{max} at 4C, and (c) ΔT

~3.6 W per cell, computed from I2R losses with internal resistance ≈ 40 mΩ) and the FS-PCM latent storage (81.5 J/g ×~12 g of composite, 7 mm thickness) predicts a buffering duration on the order of 250–300 s before the latent reservoir is exhausted. This is consistent with the experimental discharge window over which T_{max} remained <36 °C. The maximum observed reduction of 7.25 °C at 4C also corresponds qualitatively with the analytical expectation that ΔT scales inversely with the product of effective thermal conductivity and latent capacity.

5. CONCLUSION

This study presents a novel and sustainable FS-PCM synthesized from paraffin RT42 and industrial waste OA using a vacuum impregnation process for incorporation as a BTMS. Material characterization of the FS-PCM revealed physical encapsulation with retention of the original crystalline structure, thereby ensuring shape stability and leakage resistance. Additionally, SEM combined with EDS confirmed uniform paraffin infiltration and strong interfacial integration. The utilization of OA as a supporting matrix constitutes a deliberate waste valorization strategy that converts an industrial combustion byproduct into a useful battery thermal management component, thereby reducing raw material costs. The melting temperature of the resulting material (33.8 °C) was strategically matched to the upper thermal limit of safe LIB operation, ensuring uniform temperature distribution within the battery. Furthermore, the latent heat of 81.5 J/g provides meaningful thermal buffering capacity. The developed FS-PCM showed a measurable thermal conductivity enhancement over RT42. Consequently, application of the FS-PCM significantly enhanced battery thermal management by reducing the maximum device temperature by 7.25 °C at a discharge rate of 4C and maintaining temperature uniformity within safe limits. This improvement was attributed to the combined effect of the high thermal conductivity and latent heat storage, which renders the FS-PCM an effective passive cooling solution for LIBs. Moreover, increasing the FS-PCM thickness from 5 to 7 mm improved the cooling performance, highlighting the potential for practical system-level optimization. Despite these promising results, this study has several limitations. Firstly, thermal performance was evaluated at the single-cell level under controlled laboratory conditions. Thus, the module- and pack-level behaviors, where heat accumulation and intercell coupling become significant, remain to be investigated. Additionally, the long-term cycling stability, thermomechanical fatigue of the OA matrix, and potential degradation of the RT42/OA composite over hundreds of charge–discharge cycles were not assessed and remain to be quantified. Future work should, therefore, extend the present study to address these limitations to ultimately quantify the sustainability and cost benefits of OA valorization at scale. Nevertheless, the current findings establish the RT42/OA FS-PCM composite as a technically viable and economically attractive passive cooling solution for LIBs in thermally demanding environments, with particular relevance to EV deployment in hot arid climates.

AFFILIATIONS AND AUTHOR DETAILS

Undergraduate Author

Meshal Alghamdi – *Department of Mechanical Engineering, King Fahd University of Petroleum & Minerals, Dhahran 31261, Saudi Arabia*; 0009-0006-0759-6240
Email: s202153930@kfupm.edu.sa

Corresponding Author

Obaidallah Munteshari – *Research Mentor, Assistant Professor, Department of Mechanical Engineering, King Fahd University of Petroleum & Minerals, Dhahran 31261, Saudi Arabia*; 0000-0003-3587-4632
Email: obaidallah@kfupm.edu.sa

ACKNOWLEDGEMENTS

The authors would like to express their sincere gratitude to Dr. Khaled Mohaisen and Dr. Mohammad Faizan for their valuable guidance, insightful discussions, and continued support throughout this research.

REFERENCES

(1) B. Chen, R. Xiong, H. Li, Q. Sun, J. Yang, Pathways for sustainable energy transition, J. Clean. Prod. 228 (2019) 1564–1571. https://doi.org/10.1016/j.jclepro.2019.04.372.

(2) R. Bandela, F. Shaik, Modeling of Phase Change Materials in Electric Vehicle Battery Thermal Management, IOP Conf. Ser. Mater. Sci. Eng. 1334 (2025) 012007. https://doi.org/10.1088/1757-899x/1334/1/012007.

(3) S. Ali, M.M. Khan, Experimental Investigation of Battery Thermal Management System of Lithium-Ion Cells Using PCM, Engineering Proceedings 45 (2023). https://doi.org/10.3390/engproc2023045052.

(4) K. Vohra, A. Vodonos, J. Schwartz, E.A. Marais, M.P. Sulprizio, L.J. Mickley, Global mortality from outdoor fine particle pollution generated by fossil fuel combustion: Results from GEOS-Chem, Environ. Res. 195 (2021) 110754. https://doi.org/10.1016/j.envres.2021.110754.

(5) M. Irfan, M.A. Musarat, W.S. Alaloul, M. Ghufran, Radiative forcing on climate change: assessing the effect of greenhouse gases on energy balance of Earth, in: Advances and Technology Development in Greenhouse Gases: Emission, Capture and Conversion, Elsevier, 2024: pp. 137–167. https://doi.org/10.1016/B978-0-443-19066-7.00012-6.

(6) X. Xia, P. Li, Z. Xia, R. Wu, Y. Cheng, Life cycle carbon footprint of electric vehicles in different countries: A review, Sep. Purif. Technol. 301 (2022) 122063. https://doi.org/10.1016/j.seppur.2022.122063.

(7) J. Carey, The other benefit of electric vehicles, Proc. Natl. Acad. Sci. U. S. A. 120 (2023). https://doi.org/10.1073/pnas.2220923120.

(8) B. Du, H. Jia, B. Zhang, Y. Li, H. Wang, J. Yan, E. Du, N. Zhang, Evaluating the carbon-emission reduction potential of employing low-carbon demand response to guide electric-vehicle charging: A Chinese case study, Appl. Energy 397 (2025). https://doi.org/10.1016/j.apenergy.2025.126196.

(9) S. Verma, G. Dwivedi, P. Verma, Life cycle assessment of electric vehicles in comparison to combustion engine vehicles: A review, in: Mater. Today Proc., Elsevier Ltd, 2021: pp. 217–222. https://doi.org/10.1016/j.matpr.2021.01.666.

(10) B.K. Sovacool, L. Noel, J. Axsen, W. Kempton, The neglected social dimensions to a vehicle-to-grid (V2G) transition: A critical and systematic review, Environmental Research Letters 13 (2018). https://doi.org/10.1088/1748-9326/aa9c6d.

(11) M. Coffman, P. Bernstein, S. Wee, Electric vehicles revisited: a review of factors that affect adoption, Transp. Rev. 37 (2017) 79–93. https://doi.org/10.1080/01441647.2016.1217282.

(12) M. Mahmoud, The Future of Climate Change Mitigation in the Middle East and North Africa, Middle East Institute, 2023. https://www.mei.edu/publications/future-climate-change-mitigation-middle-east-and-north-africa.

(13) R. Leal-Arcas, S. Alrasheed, H. Almusaad, S.F. Alsaud, N. Alyousif, A Tale of Three Countries: Energy Decentralization in Egypt, the United Arab Emirates, and Saudi Arabia, SSRN (2024). https://doi.org/10.2139/ssrn.4997965.

(14) C. Raymond, T. Matthews, C. Tuholske, Post-Sunset Humid-Heat Maxima near the Southern Persian/Arabian Gulf, (2024). https://doi.org/10.21203/rs.3.rs-3919308/v1.

(15) H.M. Hasanean, A.H. Labban, Features of climatic temperature over Saudi Arabia: A Review, Időjárás 126 (2022) 511–543. https://doi.org/10.28974/idojaras.2022.4.4.

(16) T. Waldmann, M. Wilka, M. Kasper, M. Fleischhammer, M. Wohlfahrt-Mehrens, Temperature dependent ageing mechanisms in Lithium-ion batteries - A Post-Mortem study, J. Power Sources 262 (2014) 129–135. https://doi.org/10.1016/j.jpowsour.2014.03.112.

(17) T.M. Bandhauer, S. Garimella, T.F. Fuller, A Critical Review of Thermal Issues in Lithium-Ion Batteries, J. Electrochem. Soc. 158 (2011) R1. https://doi.org/10.1149/1.3515880.

(18) A.M. Elshurafa, N. Peerbocus, Electric vehicle deployment and carbon emissions in Saudi Arabia: A power system perspective, Electricity Journal 33 (2020). https://doi.org/10.1016/j.tej.2020.106774.

(19) S. Alotaibi, S. Omer, Y. Su, Identification of Potential Barriers to Electric Vehicle Adoption in Oil-Producing Nations—The Case of Saudi Arabia, Electricity 3 (2022) 365–395. https://doi.org/10.3390/electricity3030020.

(20) X. Zhang, Z. Li, L. Luo, Y. Fan, Z. Du, A review on thermal management of lithium-ion batteries for electric vehicles, Energy 238 (2022) 121652. https://doi.org/10.1016/j.energy.2021.121652.

(21) L. Spitthoff, P.R. Shearing, O.S. Burheim, Temperature, ageing and thermal management of lithium-ion batteries, Energies 14 (2021) 1248. https://doi.org/10.3390/en14051248.

(22) B. Fouzia, Technico-economical efficient multiyear comparative analysis of temperature and cycling effect on Li-ion and lead-acid batteries — A case study, J. Energy Storage 74 (2023). https://doi.org/10.1016/j.est.2023.109310.

(23) T. Sutikno, W. Arsadiando, H.S. Purnama, Battery types and recent developments for energy storage in electric vehicles: technical criteria and battery management system, Clean Energy 9 (2025) 293–322. https://doi.org/10.1093/ce/zkaf048.

(24) R. Yudhistira, D. Khatiwada, F. Sanchez, A comparative life cycle assessment of lithium-ion and lead-acid batteries for grid energy storage, J. Clean. Prod. 358 (2022). https://doi.org/10.1016/j.jclepro.2022.131999.

(25) S. Guo, Q. Jia, Y. Li, L. Zhang, W. Wang, S. Han, Enhanced low temperature performance of La–Mg–Ni-based superlattice structure hydrogen storage alloys for nickel-metal hydride batteries, J. Energy Storage 145 (2026). https://doi.org/10.1016/j.est.2025.119935.

(26) M. Faizan, O. Munteshari, Improved heat dissipation of high-rate lithium-ion battery using hybrid composite phase change material and nanofluid cooling. Int. J. Therm. Sci. 226 (2026) 110844. https://doi.org/10.1016/j.ijthermalsci.2026.110844.

(27) M.I. Khan, R. Gilani, J. Hafeez, R. Ayoub, I. Zahoor, G. Saira, Advantages and disadvantages of lithium-ion batteries, in: Nanostructured Lithium-Ion Battery Materials, Elsevier, 2025: pp. 47–64. https://doi.org/10.1016/B978-0-443-13338-1.00017-4.

(28) M. Walter, M. V. Kovalenko, K. V. Kravchyk, Challenges and benefits of post-lithium-ion batteries, New Journal of Chemistry 44 (2020) 1677–1683. https://doi.org/10.1039/c9nj05682c.

(29) M. Faizan, S. Pati, P. Randive, Implications of novel cold plate design with hybrid cooling on thermal management of fast discharging lithium-ion battery. J. Energy Storage 53 (2022) 105051. https://doi.org/10.1016/j.est.2022.105051.

(30) M. Faizan, S. Pati, P. Randive, Effect of channel configurations on the thermal management of fast discharging Li-ion battery module with hybrid cooling, Energy 267 (2023) 126358. https://doi.org/10.1016/j.energy.2022.126358.

(31) K. Liu, J. Wang, T. Yamamoto, T. Morikawa, Exploring the interactive effects of ambient temperature and vehicle auxiliary loads on electric vehicle energy consumption, Appl. Energy 227 (2018) 324–331. https://doi.org/10.1016/j.apenergy.2017.08.074.

(32) Y. Liu, G. Feng, S. Chang, Y. Cheng, Research on the design and hierarchical control strategy of wind-PV-energy storage and electric vehicle integrated energy systems for zero-carbon buildings, Energy Build. 345 (2025) 116032. https://doi.org/10.1016/j.enbuild.2025.116032.

(33) S. Ma, M. Jiang, P. Tao, C. Song, J. Wu, J. Wang, T. Deng, W. Shang, Temperature effect and thermal impact in lithium-ion batteries: A review, Progress in Natural Science: Materials International 28 (2018) 653–666. https://doi.org/10.1016/j.pnsc.2018.11.002.

(34) R. Srinivasan, P.A. Demirev, B.G. Carkhuff, S. Santhanagopalan, J.A. Jeevarajan, T.P. Barrera, Review—Thermal Safety Management in Li-Ion Batteries: Current Issues and Perspectives, J. Electrochem. Soc. 167 (2020) 140516. https://doi.org/10.1149/1945-7111/abc0a5.

(35) L. He, Z. Gu, Y. Zhang, H. Jing, P. Li, Review on Thermal Management of Lithium-Ion Batteries for Electric Vehicles: Advances, Challenges, and Outlook, Energy and Fuels 37 (2023) 4835–4857. https://doi.org/10.1021/acs.energyfuels.2c04243.

(36) A. Alawi, A. Saeed, M.H. Sharqawy, M. Al Janaideh, A Comprehensive Review of Thermal Management Challenges and Safety Considerations in Lithium-Ion Batteries for Electric Vehicles, Batteries 11 (2025). https://doi.org/10.3390/batteries11070275.

(37) M. Shen, Q. Gao, Structure design and effect analysis on refrigerant cooling enhancement of battery thermal management system for electric vehicles, J. Energy Storage 32 (2020). https://doi.org/10.1016/j.est.2020.101940.

(38) N. Sharifi, H. Shabgard, C. Millard, U. Etufugh, Hybrid Heat Pipe-PCM-Assisted Thermal Management for Lithium-Ion Batteries, Batteries 11 (2025). https://doi.org/10.3390/batteries11020064.

(39) S. Wankhede, A.D. Pingale, A. Kale, Experimental investigation on thermal management of lithium-ion battery pack for formula student electric vehicle using air-cooling system, Energy Storage and Saving 4 (2025) 38–47. https://doi.org/10.1016/j.enss.2024.11.008.

(40) M. Tang, C. Wu, W. Peng, R. Han, S. Zhang, D. Wang, Numerical simulation study on the impact of convective heat transfer on lithium battery air cooling thermal model, Appl. Therm. Eng. 257 (2024) 124220. https://doi.org/10.1016/j.applthermaleng.2024.124220.

(41) C. Yang, H. Xi, M. Wang, Structure optimization of air cooling battery thermal management system based on lithium-ion battery, J. Energy Storage 59 (2023) 106538. https://doi.org/10.1016/j.est.2022.106538.

(42) X.-H. Feng, Y.-L. Lou, K. Zhang, Z.-Z. Li, M.-L. Zhang, Optimization of liquid-cooled lithium-ion battery thermal management system under extreme temperature, J. Energy Storage 99 (2024) 113214. https://doi.org/10.1016/j.est.2024.113214.

(43) K. Liang, Y. Zhang, W. Wang, C. Gao, H. Chen, K. Li, X. Zhou, B. Chen, Y. Cao, W. Wang, D. Yang, L. Song, Performance analysis and multi-objective optimization of refrigerant-based integrated thermal management system for electric vehicles, Appl. Therm. Eng. 244 (2024) 122707. https://doi.org/10.1016/j.applthermaleng.2024.122707.

(44) N.C. Parker, M. Kuby, J. Liu, E.B. Stechel, Extreme heat effects on electric vehicle energy consumption and driving range, Appl. Energy 380 (2025) 125051. https://doi.org/10.1016/j.apenergy.2024.125051.

(45) Z. Li, Y. Zhang, S. Zhang, B. Tang, Phase change materials for lithium-ion battery thermal management systems: A review, J. Energy Storage 80 (2024) 110259. https://doi.org/10.1016/j.est.2023.110259.

(46) S. Rana, R. Kumar, and R.S. Bharj. Experimental and numerical investigation on the thermal performance of fin-enhanced PCM-based temperature regulation system for lithium-ion batteries, Int. J. Therm. Sci. 220 (2026) 10311. https://doi.org/10.1016/j.ijthermalsci.2025.110311.

(47) D. Zhou, C.Y. Zhao, Y. Tian, Review on thermal energy storage with phase change materials (PCMs) in building applications, Appl. Energy 92 (2012) 593–605. https://doi.org/10.1016/j.apenergy.2011.08.025.

(48) N. Joshy, M. Hajiyan, A.R.M. Siddique, S. Tasnim, H. Simha, S. Mahmud, Experimental investigation of the effect of vibration on phase change material (PCM) based battery thermal management system, J. Power Sources 450 (2020) 227717. https://doi.org/10.1016/j.jpowsour.2020.227717.

(49) C. Wu, J. Ni, X. Shi, Research on multiple thermal conductivity phase-change-material-liquid thermal management system considering thermal safety and temperature uniformity of battery pack, J. Energy Storage 136 (2025) 118456. https://doi.org/10.1016/j.est.2025.118456.

(50) Z. Wang, Z. Zhang, L. Jia, L. Yang, Paraffin and paraffin/aluminum foam composite phase change material heat storage experimental study based on thermal management of Li-ion battery, Appl. Therm. Eng. 78 (2015) 428–436. https://doi.org/10.1016/j.applthermaleng.2015.01.009.

(51) H. Yang, Y. Bai, C. Ge, L. He, W. Liang, X. Zhang, Polyethylene glycol-based phase change materials with high photothermal conversion efficiency and shape stability in an aqueous environment for solar water heater, Compos. Part A Appl. Sci. Manuf. 154 (2022) 106778. https://doi.org/10.1016/j.compositesa.2021.106778.

(52) H. Wang, Y. Guo, Y. Ren, S. Yeboah, J. Wang, F. Long, Z. Zhang, R. Jiang, Investigation of the thermal management potential of phase change material for lithium-ion battery, Appl. Therm. Eng. 236 (2024) 121590. https://doi.org/10.1016/j.applthermaleng.2023.121590.

(53) C.Y. Zhao, Z.G. Wu, Heat transfer enhancement of high temperature thermal energy storage using metal foams and expanded graphite, Solar Energy Materials and Solar Cells 95 (2011) 636–643. https://doi.org/10.1016/j.solmat.2010.09.032.

(54) Y. Lin, Y. Jia, G. Alva, G. Fang, Review on thermal conductivity enhancement, thermal properties and applications of phase change materials in thermal energy storage, Renewable and Sustainable Energy Reviews 82 (2018) 2730–2742. https://doi.org/10.1016/j.rser.2017.10.002.

(55) Z.A. Qureshi, H.M. Ali, S. Khushnood, Recent advances on thermal conductivity enhancement of phase change materials for energy storage system: A review, Int. J. Heat Mass Transf. 127 (2018) 838–856. https://doi.org/10.1016/j.ijheatmasstransfer.2018.08.049.

(56) Q. Xin, T. Yang, H. Zhang, J. Yang, J. Zeng and J. Xiao. Experimental and numerical study of lithium-ion battery thermal management system using composite phase change material and liquid cooling. J. of Energy Storage. 71 (2023). https://doi.org/10.1016/j.est.2023.108003.

(57) Z. Bian, F. Hou, Y. Bai, Q. Dong, H. Wang, Composited phase change material with hierarchical metal foam for efficient thermal energy management, Appl. Therm. Eng. 236 (2024) 121745. https://doi.org/10.1016/j.applthermaleng.2023.121745.

(58) R. Jilte, A. Afzal, Ü. Ağbulut, S. Shaik, S.A. Khan, E. Linul, M. Asif, Battery thermal management of a novel helical channeled cylindrical Li-ion battery with nanofluid and hybrid nanoparticle-enhanced phase change material, Int. J. Heat Mass Transf. 216 (2023) 124547. https://doi.org/10.1016/j.ijheatmasstransfer.2023.124547.

(59) Z. He, R. Li, L. Yang, H. Mikulčić, J. Wang, L. Čuček, Performance analysis of a battery thermal management system based on phase change materials with micro heat pipe arrays, Energy Convers. Manag. 311 (2024) 118506. https://doi.org/10.1016/j.enconman.2024.118506.

(60) P. Ping, X. Dai, D. Kong, Y. Zhang, X. Gao, W. Gao, Experimental study on nano-encapsulated inorganic phase change material for lithium-ion battery thermal management and thermal runaway suppression, Chem. Eng. J. 463 (2023) 142401. https://doi.org/10.1016/j.cej.2023.142401.

(61) A. Al Miaari, K.O. Mohaisen, R.A. Lawag, A. Al-Ahmed, H.M. Ali, Characterization of a novel sustainable shape stabilized phase change material based on OA for photovoltaic thermal management, Solar Energy 292 (2025) 113455. https://doi.org/10.1016/j.solener.2025.113455.

(62) Y. Gong, J. Zhang, Y. Chen, D. Ouyang, M. Chen, Application of Polyethylene Glycol-Based Flame-Retardant Phase Change Materials in the Thermal Management of Lithium-Ion Batteries, Polymers (Basel). 15 (2023). https://doi.org/10.3390/polym15224450.

(63) R.R. A, L. M, K. P, Thermal Control in Battery Systems: Experimental Analysis using Phase Change Materials, Journal of Electronics and Informatics 6 (2024) 292–300. https://doi.org/10.36548/jei.2024.4.001.

(64) X. Li, T. Lu, W. Liu, W. Lv, S. Lv, Ultra-wide-temperature-range thermal self-responsive phase-change materials for lithium battery thermal management, Cell Rep. Phys. Sci. 6 (2025). https://doi.org/10.1016/j.xcrp.2025.102617.

(65) N.S. Mane, P. Kodancha, V. Hemadri, S. Tripathi, Investigation on Cooling Performance of Composite PCM and Graphite Fin for Battery Thermal Management System of Electric Vehicles, Energy Storage 6 (2024). https://doi.org/10.1002/est2.70024.

(66) A.P. Avik, A.M. Kannan, V. Ruuskanen, S. Mostafaie, P. Kauranen, Passive thermal management of a Li-ion battery module using phase change materials, Appl. Therm. Eng. 288 (2026). https://doi.org/10.1016/j.applthermaleng.2025.129563.

(67) S.A. Hussien, A.B.M. Ali, O.J. Alkhatib, I. Mahariq, Enhanced passive thermal management of lithium-ion batteries with conical cylindrical chamber incorporating various phase change materials, Sci. Rep. 15 (2025). https://doi.org/10.1038/s41598-025-19597-0.

(68) A.R. Abdulmunem, H.M. Hamed, P.M. Samin, I.I. Mazali, K. Sopian, Thermal management of lithium-ion batteries using palm fatty acid distillate as a sustainable bio-phase change material, J. Energy Storage 73 (2023). https://doi.org/10.1016/j.est.2023.109187.

(69) A. Khan, M. Ali, S. Yaqub, H.A. Khalid, R.R.U. Khan, K. Mushtaq, H. Nazir, Z. Said, Hybrid thermal management of Li-ion battery pack: An experimental study with eutectic PCM-embedded heat transfer fluid, J. Energy Storage 77 (2024). https://doi.org/10.1016/j.est.2023.109929.

(70) Z. Sun, Y. Guo, C. Zhang, J. Whitehouse, Q. Zhou, H. Xu, C. Wang, Experimental study of battery passive thermal management system using copper foam-based phase change materials, International Journal of Thermofluids 17 (2023). https://doi.org/10.1016/j.ijft.2022.100255.

(71) X. Xiao, M. Yao, Y. Xu, G. Jiang, Y. Duan, Preparation and characterization of TPEE@PEG1500/EG flexible composite phase change materials and thermal response for thermal management of batteries, Energy Convers. Manag. 352 (2026) 121044. https://doi.org/10.1016/j.enconman.2026.121044.

(72) A. Al Miaari, K. Mohaisen, A. Al-Ahmed, H.M. Ali, Experimental investigation on thermal management and performance enhancement of photovoltaic panel cooled by a sustainable shape stabilized phase change material, Case Studies in Thermal Engineering (2025) 105763. https://doi.org/10.1016/j.csite.2025.105763.

(73) H. Khan, A.S. Yerramilli, A. D'Oliveira, T.L. Alford, D.C. Boffito, G.S. Patience, Experimental methods in chemical engineering: X-ray diffraction spectroscopy—XRD, Canadian Journal of Chemical Engineering 98 (2020) 1255–1266. https://doi.org/10.1002/cjce.23747.

(74) J.D. Menczel, L. Judovits, R.B. Prime, H.E. Bair, M. Reading, S. Swier, Differential Scanning Calorimetry (DSC), in: Thermal Analysis of Polymers, 2009: pp. 7–239. https://doi.org/10.1002/9780470423837.ch2.

(75) D. Tomasino, Z. Jenei, W. Evans, C.-S. Yoo, Melting and phase transitions of nitrogen under high pressures and temperatures, J. Chem. Phys. 140 (2014) 244510. https://doi.org/10.1063/1.\protect\penalty-\@M4885724.

(76) J.H. Flynn, Analysis of DSC results by integration, Thermochim. Acta 217 (1993) 129–149. https://doi.org/10.1016/0040-6031(93)85104-H.